ISSN : 1226-7244 (Print)
ISSN : 2288-243X (Online)
논문번호 21-04-10

j.inst.Korean.electr.electron.eng.Vol.25,No.4,650~663,December 2021
https://doi.org/10.7471/ikeee.2021.25.4.650

A study on estimating the interlayer boundary of the subsurface using a artificial neural network with electrical impedance tomography

Sunam Kumar Sharma*, Anil Kumar Khambampati*, Kyung Youn Kim*★

Abstract

Subsurface topology estimation is an important factor in the geophysical survey. Electrical impedance tomography is one of the popular methods used for subsurface imaging. The EIT inverse problem is highly nonlinear and ill-posed; therefore, reconstructed conductivity distribution suffers from low spatial resolution. The subsurface region can be approximated as piece-wise separate regions with constant conductivity in each region; therefore, the conductivity estimation problem is transformed to estimate the shape and location of the layer boundary interface. Each layer interface boundary is treated as an open boundary that is described using front points. The subsurface domain contains multi-layers with very complex configurations, and, in such situations, conventional methods such as the modified Newton Raphson method fail to provide the desired solution. Therefore, in this work, we have implemented a 7-layer artificial neural network (ANN) as an inverse problem algorithm to estimate the front points that describe the multi-layer interface boundaries. An ANN model consisting of input, output, and five fully connected hidden layers are trained for interlayer boundary reconstruction using training data that consists of pairs of voltage measurements of the subsurface domain with three-layer configuration and the corresponding front points of interface boundaries. The results from the proposed ANN model are compared with the gravitational search algorithm (GSA) for interlayer boundary estimation, and the results show that ANN is successful in estimating the layer boundaries with good accuracy.

Key words : Electrical impedance tomography, artificial neural network, front points, subsurface, interlayer estimation

Ⅰ. Introduction

Geophysical methods are used for exploration of petroleum, gases, groundwater, minerals and investing waste contamination as well [1]-[5]. It is also used for the investigation and understanding of the subsurface structure, layers, and composition. Ground-penetrating radar (GPR) [6] and electrical resistivity tomography (ERT) [7] are the geophysical methods used for the exploration of the subsurface. GPR method is expensive when compared with ERT for the subsurface survey.

The subsurface structures are in different shapes and, sizes and are hard to estimate in a complex environment. Subsurface is a composition of the soil, minerals, water, etc. The physics of electrical

* Department of Electronic Engineering, Jeju National University
★ Corresponding author
E-mail: kyungyk@jejunu.ac.kr, Tel : +82-64-754-3664
※ Acknowledgment
This research was supported by the 2021 scientific promotion program funded by Jeju National University Manuscript received
Manuscript received Dec. 6, 2021; revised Dec. 17, 2021; accepted Dec. 20, 2021.

current flow in the soil suggests the relationship between electrical resistivity and soil strength. The relationship between electrical resistivity and soil strength changes based on the clay content in the soil [8]. The soil moisture often influences the electrical conductivity [9], [10]. The subsurface electrical properties are generally obtained using borehole and surface measurement technique [11]. These measurement techniques are implemented either together or separately when reconstructing the electrical conductivity by electrical resistivity tomography (ERT) [12] or electrical impedance tomography (EIT).

The borehole technique is a well-based sampling method, used for direct sample collection. It provides discrete information, and more sampling wells are needed to investigate the large area. Sometimes, the wall rock can collapse into the holes if the casing is not done. Due to these reasons, the implementation of the borehole technique tends to become expensive for the implementation. Whereas in the surface measurement technique, wells are not required for the measurement. It is executed with the electrode array being placed on the surface of the domain. Since there are no wells, the surface measurement method can measure a large area in less time and cost. But to validate the output of surface measurement, few wells are drilled.

A resistivity contrast between different layers of the subsurface makes the detection and recognition possible in the electrical geophysical method. An electrical survey method is conducted by a non-invasive method known as electrical resistance tomography or electrical impedance tomography (EIT). Electrical impedance tomography (EIT) reconstructs the cross-sectional image of the conductivity distribution of the area under study [13], [14]. EIT has been implemented in many fields such as the study of petroleum product reservoir monitoring, process flow monitoring, underground pollutants, aquifer detection, breast cancer detection, lung function monitoring, and others [15]-[19]. In EIT, the electrodes are placed on the surface of the domain equidistantly. These electrodes are used to inject the current and measured the corresponding electric potential. The conductivity contrast between the different subsurface layers generates the different voltage readings on the different electrodes. This numerical calculation is normally done with the fnite element method [20]-[22] and boundary element method [23]-[26]. However, boundary element method involves additional computation of fluxes on the inclusion boundary and potential on the electrode surface; thus, it is much more computationally intensive [27] due to which finite element method is preferred.

The different voltage measurement reading obtained from numerical calculation is then used to estimate the pixel conductivity distribution of the subsurface. The material size, shape and, location in the subsurface can be estimated from the reconstructed EIT image.

Since the EIT suffers from the ill-posedness problem, reconstructed conductivity image has a low spatial resolution [28][29]. A common method to overcome the low spatial resolution of EIT is to decrease the number of unknowns to estimate with incorporating the available prior information into the solution. The conductivity distribution within the layers can be assumed as piece-wise constant and known a priori. The unknowns can be the location and shape of the interface boundary between layers. A borehole technique can be performed before the electrical survey to know the characteristics of subsurface layers. The information obtained from the borehole technique can be used as a priori information for estimating the interlayer boundary using EIT. The subsurface domain comprises disjoint layer regions separated by an interfacial boundary. The interfacial boundary between layers is described by front points [30] from the horizontal reference surface and are the unknowns to be estimated using EIT. The material conductivity

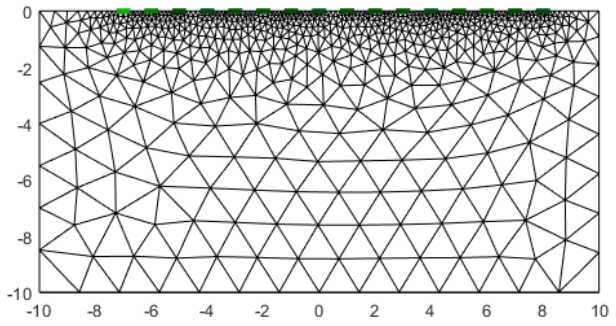

Fig. 1. A subsurface FEM mesh used in the study.

information obtained from the borehole technique can be used as a priori information for estimating the interlayer boundary using EIT. Different layers are combined to form a subsurface domain, and the interlayer boundary represents the open boundary, and the domain is divided into separate disjoint regions. Other method to defne the shape or the boundaries are also studied with electrical impedance tomography such as Fourier series [31], level set method [32], and B-spline-based method [33].

Normally, modified Newton Raphson (mNR) algorithm is used as a standard inverse solver algorithm for the EIT. An mNR algorithm heavily depends on the initial guess and the Jacobian matrix. Due to this dependency, the mNR algorithm tends to have intersecting boundaries in the complex domain. The performance of the mNR algorithm has been evaluated against gravitational search algorithm which out perform mNR [34]. Recently, the study on the artifcial neural network has increased by ten folds and has been implemented in many research work such as image recognition, natural, language processing, medical application, etc [35]. Neural Network has also been used with EIT and implemented in many research work such as estimating bladder boundary for medical application [36], estimating aquifer location for geophysics application [37], in a robotic tactile sensor [38], etc.

In this work, ANN model has been proposed as an inverse problem algorithm to estimate the interlayer boundary of the subsurface using EIT. The front points is used to define the boundary between the different layers of the subsurface. Here we assume that each layer's conductivity is homogeneous within itself. The interlayer boundary estimation of the subsurface is done using the ANN model. An ANN model is trained using a dataset containing different scenarios of the measurement voltage and the known inter-layer boundary parameters. Each sample in the dataset is generated with different front points representing the interlayer boundary and the corresponding voltage measurement reading. Unseen data of measured voltage from the surface electrodes on the subsurface domain is used to evaluate the trained ANN model.

II. Electrical Impedance Tomography

EIT is a non-invasive imaging method composed of a forward and inverse problem [39]. EIT reconstructs the cross-sectional image of the internal conductivity distribution of the domain. Finite element method (FEM) [40] is used for calculating the surface voltage measurement reading in a forward problem. For estimating the interlayer boundary of subsurface using EIT, an array L number of electrodes $e_l (l = 1, 2, \cdots, L)$ are discretely placed on the surface $\partial\Omega$. A constant amplitude current $I_l (l = 1, 2, \cdots, L)$ are injected through these electrodes on a domain Ω and resulting voltages due to internal conductivity distribution is measured on the electrode surface. The conductivity distribution $\sigma(x,y)$ is known over Ω and the corresponding electrical potential u(x, y) on the Ω is governed by partial differential equation that is determined from the Maxwell equations of electromagnetism [13], [18].

$$\nabla.(\nabla\sigma u(x,y)) = 0, (x,y) \in \Omega \quad (1)$$

To represent a realistic and accurate physical model, a complete electrode model (CEM) is used [41]. For the uniqueness and existence of the

solution, Kirchhoff's laws on the measured voltages and injected currents are needed [42], which are defined as

$$\sum_{l=1}^{L} I_l = 0, \sum_{l=1}^{L} V_l = 0 \quad (2)$$

where I_l is current injected and V_l is the measured boundary potential.

1. Forward Problem

This section describes the mathematical modeling used in this work. An electric current of constant amplitude I_l is applied to the surface electrode, and boundary voltage U_l is measured through all surface electrodes according to the known internal conductivity of the domain Ω. A finite element method (FEM) [43] discretizes the potential distribution u and the conductivity σ of the domain Ω as

$$u \approx u_h(x,y) = \sum_{i=1}^{N_n} \alpha_i \phi_i(x,y) \quad (3)$$

$$\sigma \approx \sigma_h(x,y) = \sum_{i=1}^{N_e} \sigma_i \bar{\omega}_i(x,y) \quad (4)$$

where ϕ and ω are the basis function for the electric potential and conductivity distribution, respectively and a is the nodal voltage to be determined. N_n and N_e are the number of nodes and elements in the FEM subsurface mesh. Figure 1 shows the mesh of the subsurface domain under analysis using FEM. The basis functions are chosen to ensure that the constraints defined by equation 2 is fulfilled. The linear equation of the finite element formulation is expressed as

$$Ab = f \quad (5)$$

where A is the stiffness matrix defined by equation 5, b is solution vector and f is data vector. For more details regarding FEM formulation, refer to [39]. EIDORS [44] framework is used to compute the forward solution of the EIT in the Matlab software.

2. Interlayer boundary representation

When the conductivity values of the subsurface is known a priori then the shape and location of the interlayer boundary become the unknown to be estimated. Considering the subsurface are layered, the open boundary between the two layers was approximated as a discrete front points $B_\gamma(\gamma = 1,2,...,\Gamma)$ located on the boundary [45] [30]. Here Γ defines the total number of front points, which describes the interlayer boundary. The front point location B_γ is given by

$$B_\gamma = (x_\gamma, y_\gamma),\ \gamma = 1,2,...,\Gamma \quad (6)$$

where x_γ is the reference point located on the surface of the domain as shown in the figure 2. The front point y_γ is defined as the vertical distance from the reference point $(x_\gamma, 0)$ located on the surface of the domain and the unknown parameter is

$$y = (y_1, y_2, ..., y_\Gamma)^T \quad (7)$$

III. GRAVITATIONAL SEARCH ALGORITHM

This section briefly describe the gravitational search algorithm (GSA). The GSA is iterative algorithm based on the Newton gravity law and motion law. In GSA solutions are considered as an agent, and their masses measure their performance. The gravity law describes that each agent is attracted with each other by gravitational force,

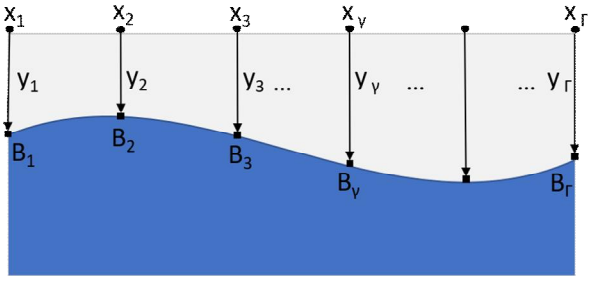

Fig. 2. Interlayer boundary parameterized with the discrete front points.

which is defined as

$$G_{i,j}(t) = g(t)\frac{M_i \times M_j}{R_{ij}+\epsilon}(y_j - y_i) \quad (8)$$

where g(t) is gravitational constant, Mi and Mj is gravitational mass of agent i and j, receptively. The position of the agents are updated based on the velocity as

$$v(t+1) = rand \times v(t) + a(t) \quad (9)$$

$$y(t+1) = y(t) + v(t+1) \quad (10)$$

where a(t) is the acceleration, v(t) is the velocity, and rand is the random number. The in-depth details of the GSA is explained in [46].

IV. ANN MODEL FOR INTERLAYER BOUNDARY ESTIMATION

This section describes how artificial neural network (ANN) model is used to estimate the interlayer boundary of the subsurface. The inverse problem estimates the internal conductivity distribution of the subsurface using the voltage reading measured from the surface electrodes and the injected current. The internal conductivity distribution of the subsurface domain reconstructed by EIT is a non-linear and ill-posed problem. These problems cause a poor spatial resolution in the reconstructed conductivity profile. To improve the reconstruction performance, number of unknowns for estimation needs to be decrease. If the conductivity values inside the subsurface domain is known as a priori, then the inverse problem of EIT becomes a shape estimation problem. In the shape estimation there are very few unknowns to be estimated which will increase the reconstruction performance and the spatial resolution.

In this work, the interlayer boundary's front points inside the subsurface domain are estimated by the artificial neural network (ANN) model. ANN model estimates the shape, size, and location of the interlayer boundary, which maps the non-linear relationship. The dataset is used to train and test the model with fully connected hidden layers with a hyperbolic tangent (Tanh) and rectified linear unit (ReLU) as the activation function [47]. This dataset contains measured voltages and related interlayer boundary front points. The ANN model comprises an input layer, output layer, and five fully connected hidden layers as illustrated in figure 3.

To estimate the interlayer boundary front points by ANN model, we define the input layer neurons as surface voltage measurements and the output layer neurons as front points. The hidden layers are used to extract the features from the training dataset, which is used to map the relationship between input and output data. The mapping function $H_\theta(v)$ is learned during the training of the model and expressed as

$$H_\theta(\nu) = \sum_{k=0}^{m} \theta^k \nu^k = \theta^T \nu \quad (11)$$

where θ is the weight of the node, ν is the measurement voltage reading, and m is the total number of data samples. In the proposed model, two different activation functions have been implemented. The first four hidden layers use the tanh function whereas, the last hidden layer is activated using ReLU function. The tanh function and ReLU function is defined as

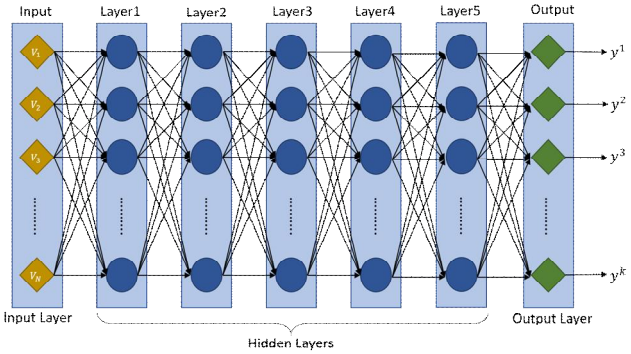

Fig. 3. Schematic diagram of the artificial neural network model. Voltage measurements reading (V1,V2,..., VN) and front points (y1, y2,..., yk) are used as input and output data, respectively.

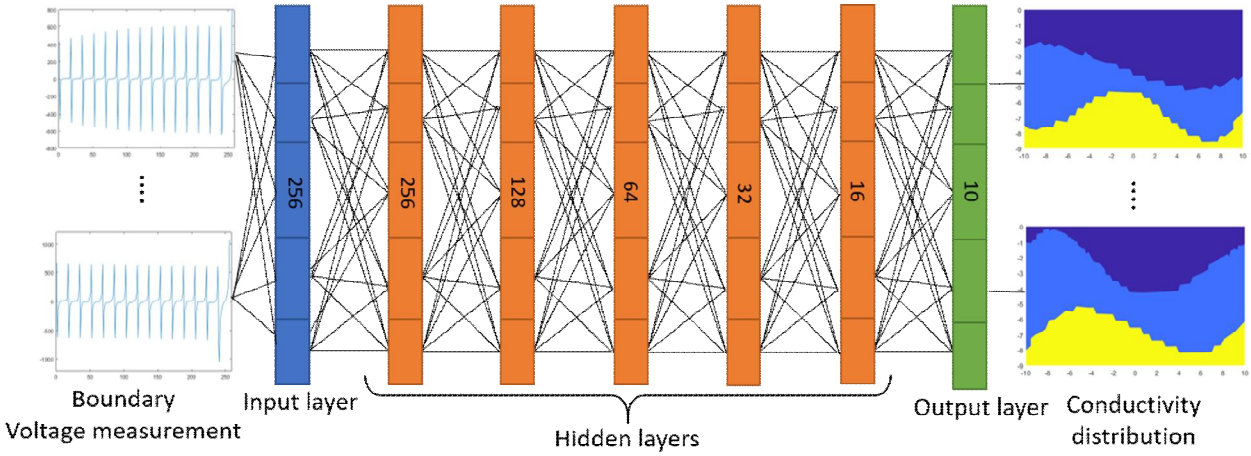

Fig. 4. Training scheme of the deep neural network model for estimating the front points of the interlayer boundaries. The number represents the number of nodes for each layers. Different voltage measurement reading and corresponding boundary front points used for as a training dataset.

$$f(\nu)=\frac{e^{\nu}-e^{-\nu}}{e^{\nu}+e^{-\nu}} \tag{12}$$

$$f(\nu)=\max(0,\nu) \tag{13}$$

The ANN model is trained to learn the weights (θ) of the nodes of the hidden layers. The training of the model for learning weights of the nodes is done by minimizing the cost function. The cost function is expressed as

$$\zeta=\frac{1}{m}\sum_{k=1}^{m}(H(v^k)-y^{k_\gamma})^2 \tag{14}$$

where m is the total number of data samples, $H(v^k)$ is the ANN predicted output and y_γ^k is the desired output of the k^{th} sample. It expresses the sum of the errors between the estimated output of the ANN model and the desired output in the ANN model. The least-square cost function is minimized to determine the weights of the node, which is expressed as

$$\theta=\arg_\theta\min\sum_{k=1}^{m}\parallel H(v^k)-y_\gamma^k\parallel^2 \tag{15}$$

The ANN model updates the weights of each nodes which minimizes the cost function. The update of the weights is executed using Adam's optimization algorithm [48]. The weights θ are updated as

$$\theta_{t+1}=\theta_t-\alpha\frac{d\zeta(\theta)}{\sqrt{\phi_t+\epsilon}} \tag{16}$$

where α is the learning rate, ϕ_t is the hyperparameter, and ϵ is a small value.

The weights, θ, are updated by ANN model during training which uses the training dataset. The trained ANN model is evaluated with unseen test data. The dataset was generated using the subsurface finite element mesh with subsurface layers, and the dataset contains the surface voltage measurement from the simulations of different shapes of the layers.

V. Result and discussion

ANN model is designed, trained, and evaluated for estimating the interlayer boundary front points inside the subsurface domain. The domain used for the study has the size of 10m in depth and 20m in width. A total of 16 surface electrodes are attached to the domain, illustrated in figure 1. These electrodes are located on top of the subsurface domain representing a surface electrode placed 1m apart. An adjacent current pattern is used in this study which generates 256 independent voltage readings.

EIT forward problem is solved using finite element method to compute the boundary voltages

for the resistivity profile with multi layer boundaries represented using front points. The three layers in the subsurface domain are assumed as alluvium, clay, and argillite. The conductivity of those layers are 0.0013 S/m, 0.01 S/m, and 0.04 S/m, respectively [9], [49]. The three layers are separated by two interlayer boundaries that have difference shapes and thickness. Each layer boundary is represented using five front points with linear interpolation.

The interlayer boundaries are considered non-crossing boundaries, and layers are considered a piece wise with constant conductivity. The bottom layer is considered as argillite, the middle layer as clay, and the top layer as alluvium. A continuous amplitude current of 1Amp is injected into the domain, and the surface voltage is measured across all surface electrodes. EIDORS [44] is used for FEM numerical calculation which generates voltage measurement reading based on the corresponding interlayer boundaries front-points of the subsurface domain. These voltage measurement reading and the corresponding front-points makes a dataset (training and testing). The training dataset is used to train the ANN model for learning the relationship between measured voltage reading and the interlayer boundary front points. The testing dataset is used to validate the training of the ANN model.

The ANN model is designed with 7-layers consisting of an input layer, five hidden layers, and an output layer as illustrated in figure 3. The node size for the input layer is based according to the voltage reading data and is set to 256. The number of nodes for the output layer is considered as 10. The output layers give the front points of the interlayer boundaries. The nodes for the hidden layers are 256, 128, 64, 32, and 16. The one training dataset sample consists of 256 independent boundary voltage measurements as input, and the corresponding output consists of 10 front points reading corresponding to the interlayer boundaries. The training scheme for the model is illustrated in figure 4. Tensorflow [50] library in python is used to implement the ANN algorithm with mean square error (MSE) as loss function and Adam optimization algorithm for optimization on a workstation configured with Intel(R) Core(TM) i7-6700 CPU @ 3.40GHz, 8GB RAM, NVIDIA GForce GT730 GPU, Windows 10. The ANN model is trained on a 20,000 dataset samples with 330 epochs and a batch size of 100. The learning rate used during the training of the ANN model is $1e^{-6}$. A validation dataset is used to validate the training process, and it contains 20% of the training dataset samples. Root mean square error (RMSE) is used to evaluate the accuracy of the trained model. The definition of RMSE is

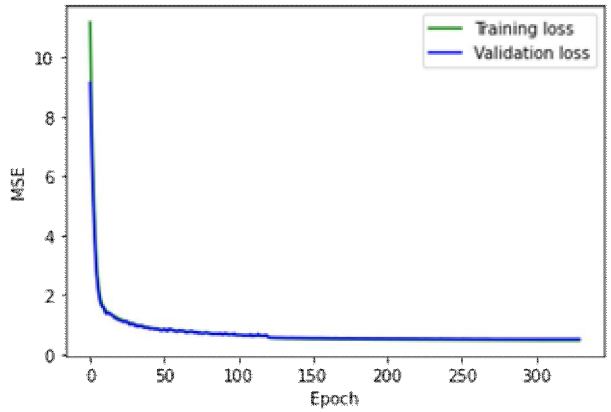

Fig. 5. Mean square error (MSE) per epoch of training and validation data during training of the DNN model.

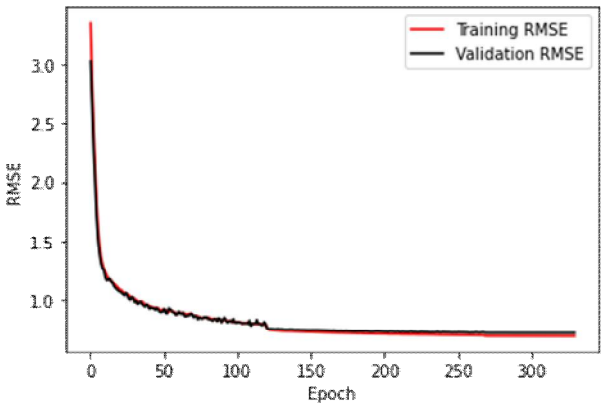

Fig. 6. Root mean square error (RMSE) per epoch of training and validation data during training of DNN model.

$$E=\sqrt{\frac{1}{N}\sum_{i=1}^{N}\left[\frac{(y_i^t-y_i)^T(y_i^t-y_i)}{(y_i^t)^T(y_i^t)}\right]} \tag{17}$$

where y is the estimated front points by ANN model and yt is the true value of front points representing the interlayer boundary in the subsurface domain. RMSE is also used for checking the error between estimated front-points with the actual front-points of the interlayer. Also, the Pearson correlation coefficient (PCC) [51] is used to find the correlation between the estimated front points and the true front points that represent interlayer boundaries. PCC is defined as

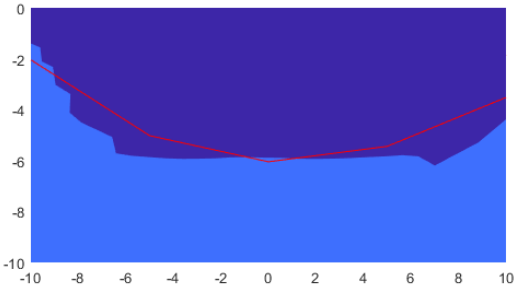

Fig. 7. True conductivity distribution of the two-layered subsurface and the estimated interlayer boundary by the GSA represented by a red line.

$$r=\frac{\sum_{i=1}^{N}(y_i-\bar{y})\sum_{i=1}^{N}(y_i^t-\bar{y^t})}{\sqrt{\sum_{i=1}^{N}(y_i-\bar{y})^2\sum_{i=1}^{N}(y_i^t-\bar{y^t})^2}} \tag{18}$$

where y is the estimated, y^t is the true value of the front points respectively, and N is the total number of front points.

The training and the validation updates per epoch of the ANN model is evaluated based on MSE and RMSE. Figure 5 show the MSE per epoch during the training of the ANN model. MSE per epoch shows the ANN model learning capability. The learning parameters are analyzedduring the training process with the validation dataset. The accuracy of the ANN model per epoch is validated using the RMSE during the training process. Figure 6 shows the RMSE per epoch during the training process. From the MSE and RMSE graphs, we can see the model's training, which has significantly improved per epoch.

When the training and validation are complete, different voltage measurement reading is used for testing. This dataset contains noisy voltage measurement readings that are unseen by the ANN model. The measurement voltage reading for every case is generated with different interlayer boundary front points. In the test cases, rocks are added to the subsurface domain into different layers and are considered while generating the test data. These rocks act as anomalies and are randomly generated for each case, considered noise in the dataset, representing a more realistic scenario. We tried to consider all types of rocks in the study that are found in the subsurface domain. The conductivities of these rocks are considered within a range of 2e-4S/m to 2e-7S/m [49].

In this work, three test cases are analyzed with different interlayer boundaries of the subsurface domain. Before comparing the GSA algorithm with the ANN, a single interlayer boundary was estimated by GSA. The estimation of the interlayer boundary for the two-layered subsurface domain was conducted before it was tested for the three-layered subsurface domain. The estimation result of the GSA and the true scenario is presented in the figure 7. The figure shows the estimated interlayer boundary by GSA has good accuracy with the ground truth.

The case 1 scenario of the subsurface is shown in figure 8a. In this case, the interlayer boundaries are linear. The anomalies represented as rocks are randomly generated and spread across the middle and lower layers of the subsurface. The reconstructed interlayer boundaries by the ANN model and the GSA for case 1 are presented in figure 8b. The estimated interlayer boundaries by the ANN model are in close resemblance to the actual scenario, whereas the estimated boundaries by GSA intersect with each other.

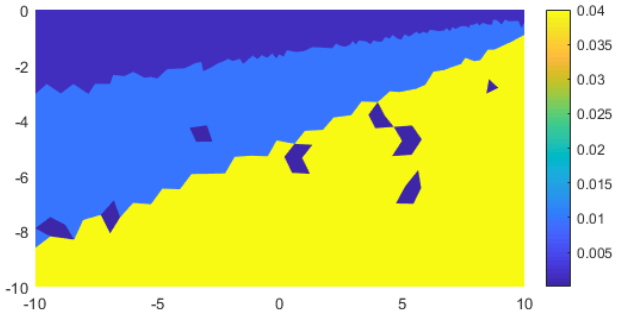

Fig. 8 a. Numerical case 1 for interlayer boundary estimation of subsurface true conductivity profile.

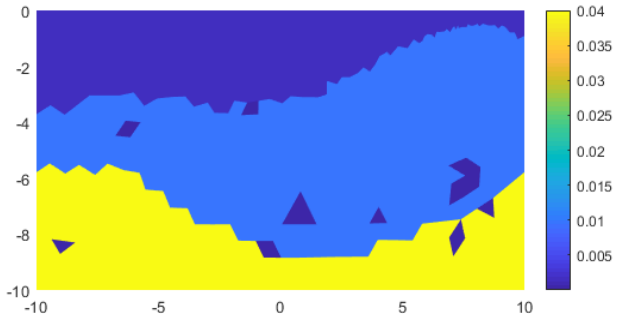

Fig. 9 a. Numerical case 2 for interlayer boundary estimation of subsurface true conductivity profile.

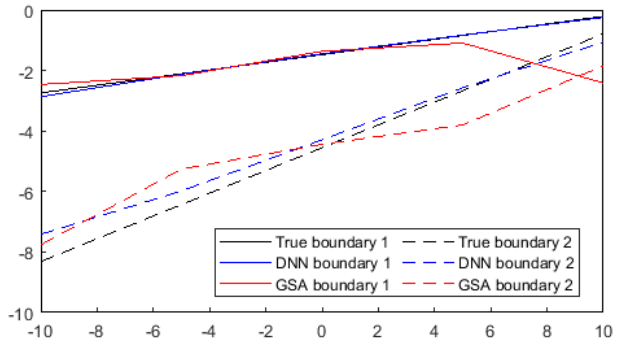

Fig. 8 b. Numerical results of case 1 for interlayer boundary estimation of subsurface reconstructed boundaries using ANN and GSA. The top, middle, and bottom layers are considered as Argellite, clay, and alluvium, respectively.

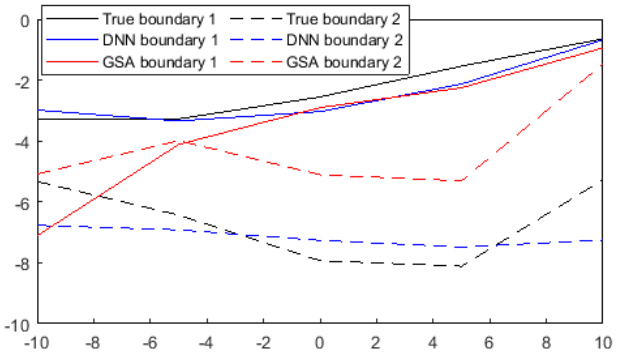

Fig. 9 b. Numerical results of case 2 for interlayer boundary estimation of subsurface reconstructed boundaries using ANN and GSA. The top, middle, and bottom layers are considered as Argellite, clay, and alluvium, respectively.

The interlayer boundaries are considered as a non-linear for the case 2. The anomalies were concentrated in the middle and bottom layers of the subsurface as shown in figure 9a. The interlayer boundary estimated by the ANN model is shown in the figure 9b. The interlayer boundaries estimated by the GSA are presented and can be compared with the ANN. Estimated boundaries by GSA are crossed or overlapped with each other, whereas ANN estimation have a good accuracy with the true interlayer boundaries.

Figure 10a shows the case 3 of the subsurface domain. In this case, the open boundaries are curved and the rocks are present in the top and the middle layers of the domain. The estimated interlayer boundaries by the ANN and the GSA algorithm are present in figure 10b. GSA failed to estimate the interlayer boundaries and are estimated close to the center region with intersected boundaries. These boundaries are overlapped and has very poor accuracy. The estimated interlayer boundaries by the ANN model, on the other hand, resemble the true case with reasonable accuracy.

From the cases studied in this work, the estimation of the interlayer boundaries front-points by ANN model has good accuracy while GSA fails to estimate the front points with good accuracy in the complex subsurface domain. The RMSE and PCC were evaluated for the front-points of the interlayer boundaries of each case estimated by both algorithms. The RMSE and PCC values are presented in table 1 and table 2, respectively. From the RMSE and PCC values, we can see that the ANN model outperformed the GSA. Of all the test cases, it is noticed that ANN has better estimation performance when the layer boundaries are linear and as the boundaries are

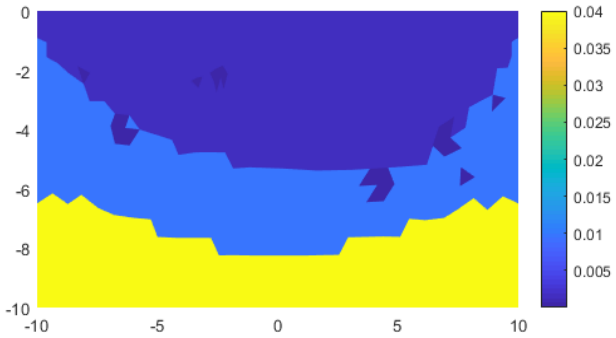

Fig. 10 a. Numerical case 3 for interlayer boundary estimation of subsurface true conductivity profile.

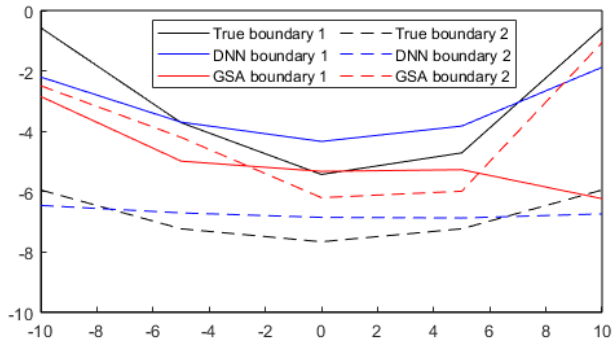

Fig. 10 b. Numerical results of case 3 for interlayer boundary estimation of subsurface reconstructed boundaries using ANN and GSA. The top, middle, and bottom layers are considered as Argellite, clay, and alluvium, respectively.

more curved the estimation is slightly affected.

The trained ANN model for estimating the front-points of open interlayer boundaries in the subsurface domain has a very good accuracy with the true scenario. However, there are limitations of this approach. The number of layers in the subsurface are assumed to be known a priori. The conductivity distribution is assumed to be uniform within each layer and the value of the layers conductivity is known beforehand also. The training of the ANN model takes time, but once the model is trained estimation of inter layer boundaries is done in few seconds. The ANN model works very well for the opened interlayer boundary but with some limitations. This ANN model is not trained for the closed interlayer boundaries and for the horizontal opened boundaries. Also, layer boundaries need to be end to end and do not intersect with each other.

Table 1. RMSE values for cases estimated by ANN and GSA.

Algorithm	Case1	Case2	Case3
ANN	0.088	0.180	0.176
GSA	0.356	0.453	0.544

Table 2. Comparison of PCC for the estimated front points by ANN and GSA.

Algorithm	Case1	Case2	Case3
ANN	0.998	0.941	0.933
GSA	0.837	0.510	0.019

Ⅵ. Conclusions

In this work, we have estimated the interlayer boundaries of subsurface using electrical impedance tomography. The conductivities inside the subsurface are assumed to be known, and the ANN model estimates the interlayer boundary. The layers a opened and are present across the domain. This ANN model is not trained for the closed and/or horizontal interlayer boundaries. Discrete front points describe the interlayer boundary. An inverse problem of estimating the interlayer boundary front points is done with a ANN model. The 7-layer ANN model is used for the estimation of front points. The ANN model is trained using the pair of boundary voltage readings and the corresponding front points. The measured voltage readings are used as an input, and interlayer boundary front points are used as output, making the dataset. The dataset is divided into three parts, i.e. training, validation, and testing, containing non-repeated data samples. A noisy measured boundary voltage is fed to a trained ANN model to estimate the corresponding interlayer boundary front points. The interlayer boundaries for subsurface estimation is done with ANN, and the performance of the proposed ANN is compared against GSA. GSA was found to have reasonable accuracy with a single-layer interface (two-layer configuration), and its performance degrades for multi-layer boundary estimation.

The performance of GSA is dependant on the number of unknowns and the range of initial solutions. The RMSE values of the estimated interlayer boundaries by the ANN model also indicate that the estimated interlayer boundaries have good accuracy than the GSA. The only drawback of the ANN model is the training time. To train a model lot of time and computing resources are needed, but the trained model estimates the parameter is a fraction of seconds. At the same time, GSA takes a lot of time to estimate the solution compared with the trained ANN model. Advantages of the ANN model are the simplicity of implementation, better accuracy and, faster estimation, and it does not require Jacobian matrix computation.

References

[1] P. Kearey, M. Brooks, and I. Hill, *An introduction to geophysical exploration*. John Wiley & Sons, vol.4, 2002.

[2] R. Philp and P. Crisp, "Surface geochemical methods used for oil and gas prospecting－a review," *Journal of Geochemical Exploration*, vol.17, no.1, pp.1-34, 1982.
DOI: 10.1016/0375-6742(82)90017-6

[3] R. Saad, M. Nawawi, and E. Mohamad, "Groundwater detection in alluvium using 2-d electrical resistivity tomography (ert)," *Electronic Journal of Geotechnical Engineering*, vol.17, pp.369-376, 2012.

[4] D. B. Hoover, D. P. Klein, D. C. Campbell, and E. du Bray, "Geophysical methods in exploration and mineral environmental investigations," *Preliminary compilation of descriptive geoenvironmental mineral deposit models:* USGS Open-File Report, vol.95, no.831, pp.1-27, 1995.

[5] N. Abdullahi, I. Osazuwa, P. Sule et al., "Application of integrated geophysical techniques in the investigation of groundwater contamination: A case study of municipal solid waste leachate," *Ozean Journal of applied sciences*, vol.4, no.1, pp.7-25, 2011.

[6] G. S. Baker, T. E. Jordan, J. Pardy et al., "An introduction to ground penetrating radar (gpr)," *Special Papers-Geological Society of America,* vol.432, p.1, 2007. DOI: 10.1130/2007.2432(01)

[7] W. Daily, A. Ramirez, D. LaBrecque, and J. Nitao, "Electrical resistivity tomography of vadose water movement," *Water Resources Research,* vol.28, no.5, pp.1429-1442, 1992.
DOI: 10.1029/91WR03087

[8] K. Sudha, M. Israil, S. Mittal, and J. Rai, "Soil characterization using electrical resistivity tomography and geotechnical investigations," *Journal of Applied Geophysics*, vol.67, no.1, pp.74-79, 2009. DOI: 10.1016/j.jappgeo.2008.09.012

[9] T. J. Katsube, P. K. Keating, H. McNairn, Y. Das, R. DiLabio, V. Singhroy, S. Connell-Madore, M. E. Best, J. Hunter, R. Klassen et al., "Soil moisture and electrical conductivity prediction and their implication for landmine detection technologies," in *Detection and Remediation Technologies for Mines and Minelike Targets IX*, vol. 5415. International Society for Optics and Photonics, pp.691-704, 2004.
DOI: 10.1117/12.542521.short?SSO=1

[10] T. J. Katsube, R. A. Klassen, Y. Das, R. Ernst, T. Calvert, G. Cross, J. Hunter, M. Best, R. DiLabio, and S. Connell, "Prediction and validation of soil electromagnetic characteristics for application in landmine detection," in *Detection and Remediation Technologies for Mines and Minelike Targets VIII*, vol.5089. International Society for Optics and Photonics, pp.1219-1230, 2003. DOI: 10.1117/12.486983.short

[11] W. Menke, "The resolving power of cross-borehole tomography," *Geophysical Research Letters,* vol.11, no.2, pp.105-108, 1984.
DOI: 10.1029/GL011i002p00105

[12] M. Perri, G. Cassiani, I. Gervasio, R. Deiana, and A. Binley, "A saline tracer test monitored via both surface and cross-borehole electrical resistivity tomography: Comparison of time-lapse results," *Journal of Applied Geophysics*, vol.79,

pp.6-16, 2012. DOI: 10.1016/j.jappgeo.2011.12.011
[13] J. G. Webster, *Electrical impedance tomography*. Taylor & Francis Group, 1990.
[14] M. Cheney, D. Isaacson, and J. C. Newell, "Electrical impedance tomography," *SIAM review*, vol.41, no.1, pp.85-101, 1999.
DOI: 10.21037/atm.2017.12.06
[15] G. D'Antona, A. Ferrero, M. Lazzaroni, R. Ottoboni, and E. Samarani, "Active monitoring apparatus for underground pollutant detection based on electrical impedance tomography," in IMTC/2002. *Proceedings of the 19th IEEE Instrumentation and Measurement Technology Conference (IEEE Cat. No. 00CH37276)*, vol.1. pp.577-579, 2002. DOI: 10.1109/IMTC.2002.1006906
[16] R. Stacey, K. Li, R. N. Horne et al., "Electrical impedance tomography (eit) technique for real-time saturation monitoring," in *SPE Annual Technical Conference and Exhibition*. Society of Petroleum Engineers, 2006. DOI: 10.2118/103124-MS
[17] A. Adler, J. H. Arnold, R. Bayford, A. Borsic, B. Brown, P. Dixon, T. J. Faes, I. Frerichs, H. Gagnon, Y. Garber ¨ et al., "Greit: a unifed approach to 2d linear eit reconstruction of lung images," *Physiological measurement,* vol.30, no.6, p.S35, 2009. DOI: 10.1088/0967-3334/30/6/S03
[18] D. Holder, "Electrical impedance tomography (eit) of brain function," *Brain Topography*, vol.5, no.2, pp.87-93, 1992. DOI: 10.1007/BF01129035
[19] E. K. Murphy, A. Mahara, X. Wu, and R. J. Halter, "Phantom experiments using soft-prior regularization eit for breast cancer imaging," *Physiological measurement*, vol.38, no.6, p.1262, 2017. DOI: 10.1088/1361-6579/aa691b
[20] A. P. Bagshaw, A. D. Liston, R. H. Bayford, A. Tizzard, A. P. Gibson, A. T. Tidswell, M. K. Sparkes, H. Dehghani, C. D. Binnie, and D. S. Holder, "Electrical impedance tomography of human brain function using reconstruction algorithms based on the fnite element method," *NeuroImage,* vol.20, no.2, pp.752-764, 2003.
DOI: 10.1016/S1053-8119(03)00301-X
[21] G. Xu, H. Wu, S. Yang, S. Liu, Y. Li, Q. Yang, W. Yan, and M. Wang, "3-d electrical impedance tomography forward problem with fnite element method," *IEEE transactions on magnetics,* vol.41, no.5, pp.1832-1835, 2005.
DOI: 10.1109/TMAG.2005.846503
[22] E. Woo, P. Hua, J. Webster, and W. Tompkins, "Finite-element method in electrical impedance tomography," *Medical and Biological Engineering and Computing,* vol.32, no.5, pp.530-536, 1994.
DOI: 10.1007/BF02515311
[23] J. C. de Munck, T. J. Faes, and R. M. Heethaar, "The boundary element method in the forward and inverse problem of electrical impedance tomography," *IEEE transactions on Biomedical Engineering,* vol.47, no.6, pp.792-800, 2000.
DOI: 10.1109/10.844230
[24] M. Tarvainen, M. Vauhkonen, T. Savolainen, and J. P. Kaipio, "Boundary element method and internal electrodes in electrical impedance tomography," *International journal for numerical methods in engineering*, vol.50, no.4, pp.809-824, 2001.
[25] R. Duraiswami, G. L. Chahine, and K. Sarkar, "Boundary element techniques for effcient 2-d and 3-d electrical impedance tomography," *Chemical engineering science*, vol.52, no.13, pp.2185-2196, 1997.
[26] R. G. Aykroyd and B. A. Cattle, "A boundary-element approach for the complete-electrode model of eit illustrated using simulated and real data," *Inverse Problems in Science and Engineering,* vol.15, no.5, pp.441-461, 2007.
DOI: 10.1080/17415970600795337
[27] A. K. Khambampati, B. A. Lee, K. Y. Kim, and S. Kim, "An analytical boundary element integral approach to track the boundary of a moving cavity using electrical impedance tomography," *Measurement Science and Technology,* vol.23, no.3, p.035401, 2012.
DOI: 10.1088/0957-0233/23/3/035401
[28] W. R. Lionheart, "Eit reconstruction algorithms: pitfalls, challenges and recent developments," *Physiological measurement,* vol.25, no.1, p.125, 2004. DOI: 10.1088/0967-3334/25/1/021

[29] E. Beretta, S. Micheletti, S. Perotto, and M. Santacesaria, “Reconstruction of a piecewise constant conductivity on a polygonal partition via shape optimization in eit,” *Journal of Computational Physics,* vol.353, pp.264-280, 2018.

[30] S. Kim, U. Z. Ijaz, A. K. Khambampati, K. Y. Kim, M. C. Kim, and S. I. Chung, “Moving interfacial boundary estimation in stratifed ?ow of two immiscible liquids using electrical resistance tomography,” *Measurement Science and Technology,* vol.18, no.5, p.1257, 2007.

[31] A. K. Khambampati, S. K. Konki, Y. Han, S. Sharma, and K. Y. Kim, “An effcient method to determine the size of bladder using electrical impedance tomography,” in *TENCON 2018~2018 IEEE Region 10 Conference*. IEEE, 2018, pp. 1933-1936.

[32] D. Liu, A. K. Khambampati, and J. Du, “A parametric level set method for electrical impedance tomography,” *IEEE transactions on medical imaging,* vol.37, no.2, pp.451-460, 2017.

[33] D. Liu, D. Gu, D. Smyl, J. Deng, and J. Du, “B-spline-based sharp feature preserving shape reconstruction approach for electrical impedance tomography,” *IEEE transactions on medical imaging,* vol.38, no.11, pp.2533-2544, 2019.

[34] S. K. Sharma, S. K. Konki, A. K. Khambampati, and K. Y. Kim, “Bladder boundary estimation by gravitational search algorithm using electrical impedance tomography,” *IEEE Transactions on Instrumentation and Measurement,* vol.69, no.12, pp.9657-9667, 2020.

[35] W. Liu, Z. Wang, X. Liu, N. Zeng, Y. Liu, and F. E. Alsaadi, “A survey of deep neural network architectures and their applications,” *Neurocomputing,* vol.234, pp.11-26, 2017.
DOI: 10.1016/j.neucom.2016.12.038

[36] S. K. Konki, A. K. Khambampati, S. K. Sharma, and K. Y. Kim, “A deep neural network for estimating the bladder boundary using electrical impedance tomography,” *Physiological Measurement,* vol.41, no.11, p.115003, 2020.
DOI: 10.1088/1361-6579/abaa56

[37] S. K. Sharma, A. K. Khambampati, and K. Y. Kim, “Estimating aquifer location using deep neural network with electrical impedance tomography,” *Journal of IKEEE,* vol.24, no.4, pp.982-990, 2020.
DOI: 10.7471/ikeee.2020.24.4.982

[38] H. Park, K. Park, S. Mo, and J. Kim, “Deep neural network based electrical impedance tomographic sensing methodology for large-area robotic tactile sensing,” *IEEE Transactions on Robotics,* 2021.
DOI: 10.1109/IROS40897.2019.8968532

[39] M. Vauhkonen, “Electrical impedance tomography and prior information [ph. d. thesis],” *University of Kuopio, Kuopio, Finland*, 1997.
DOI: 10.1.1.208.9639

[40] O. C. Zienkiewicz and R. L. Taylor, Finite Element Method: Vol. 3: *Fluid Dynamics*. Elsevier Science & Technology Books, 2000.

[41] K.-S. Cheng, D. Isaacson, J. Newell, and D. G. Gisser, “Electrode models for electric current computed tomography,” *IEEE Transactions on Biomedical Engineering,* vol.36, no.9, pp.918-924, 1989. DOI: 10.1109/10.35300

[42] E. Somersalo, M. Cheney, and D. Isaacson, “Existence and uniqueness for electrode models for electric current computed tomography,” *SIAM Journal on Applied Mathematics,* vol.52, no.4, pp.1023-1040, 1992. DOI: 10.1137/0152060

[43] S. Brenner and R. Scott, *The mathematical theory of finite element methods*. Springer Science & Business Media, vol.15, 2007.

[44] A. Adler and W. R. Lionheart, “Uses and abuses of eidors: an extensible software base for eit,” *Physiological measurement*, vol.27, no.5, p.S25, 2006. DOI: 10.1088/0967-3334/27/5/S03

[45] A. K. Khambampati, Y. J. Hong, K. Y. Kim, and S. Kim, “A boundary element method to estimate the interfacial boundary of two immiscible stratifed liquids using electrical resistance tomography,” *Chemical Engineering Science,* vol.95, pp.161-173, 2013. DOI: 10.1016/j.ces.2013.03.018

[46] E. Rashedi, H. Nezamabadi-Pour, and S. Saryazdi, “Gsa: a gravitational search algorithm,” *Information sciences,* vol.179, no.13, pp.2232-2248,

2009. DOI: 10.1016/j.ins.2009.03.004
[47] M. M. Lau and K. H. Lim, "Review of adaptive activation function in deep neural network," in 2018 *IEEE-EMBS Conference on Biomedical Engineering and Sciences (IECBES).* IEEE, pp.686-690, 2018. DOI: 10.1109/IECBES.2018.8626714
[48] D. P. Kingma and J. Ba, "Adam: A method for stochastic optimization," *arXiv preprint arXiv*:1412.6980, 2014.
[49] J. McNeill, "Electrical conductivity of soils and rocks. geonics limited," *Mississauga, Ontario, Technical Note* TN-5, 1980.
[50] M. Abadi, P. Barham, J. Chen, Z. Chen, A. Davis, J. Dean, M. Devin, S. Ghemawat, G. Irving, M. Isard et al., "Tensor?ow: A system for large-scale machine learning," in *12th {USENIX} symposium on operating systems design and implementation* ({OSDI} 16), pp.265283, 2016. DOI: 10.5555/3026877.3026899
[51] J. Lee Rodgers and W. A. Nicewander, "Thirteen ways to look at the correlation coeffcient," *The American Statistician,* vol.42, no.1, pp.59-66, 1988. DOI: 10.1080/00031305.1988.10475524

BIOGRAPHY

Sunam Kumar Sharma (Member)

2006 : BE degree in Electronics and Communication Engineering, Pokhara University, Nepal.
2016 : MS degree in Information Technology, Sikkim Manipal University, India.

Anil Kumar Khambampati (Member)

2003 : BS degree in Mechanical Engineering, Jawaharlal Nehru Technological University, India.
2006 : MS degree in Marine Instrumentation Engineering, Jeju National University.
2010 : PhD degree in Electronic Engineering, Jeju National University.

Kyung Youn Kim (Member)

1983 : BS degree in Electronic Engineering, Kyungpook National University.
1986 : MS degree in Electronic Engineering, Kyungpook National University.
1990 : PhD degree in Electronic Engineering, Kyungpook National University.